AGU PUBLICATIONS

Water Resources Research

RESEARCH ARTICLE
10.1002/2014WR016369

Key Points:
- Density effect constrains solute release from riverbed
- Density effect and solute tranport lead to a long tail in river water
- High solute concentration contrasts lead to unstable flow in riverbed

Supporting Information:
- Supporting Information S1

Correspondence to:
H. Tang,
hwtang@hhu.edu.cn

Citation:
Jin, G., H. Tang, L. Li, and D. A. Barry (2015), Prolonged river water pollution due to variable-density flow and solute transport in the riverbed, *Water Resour. Res.*, *51*, 1898–1915, doi:10.1002/2014WR016369.

Received 8 SEP 2014
Accepted 4 FEB 2015
Accepted article online 10 FEB 2015
Published online 2 APR 2015

Prolonged river water pollution due to variable-density flow and solute transport in the riverbed

Guangqiu Jin[1], Hongwu Tang[1], Ling Li[1,2], and D. A. Barry[3]

[1]State Key Laboratory of Hydrology-Water Resources and Hydraulic Engineering, Hohai University, Nanjing, China, [2]School of Civil Engineering, University of Queensland, Queensland, Australia, [3]Laboratoire de technologie écologique, Institut d'ingénierie de l'environnement, Faculté de l'environnement naturel, architectural et construit, Ecole Polytechnique Fédérale de Lausanne, Lausanne, Switzerland

Abstract A laboratory experiment and numerical modeling were used to examine effects of density gradients on hyporheic flow and solute transport under the condition of a solute pulse input to a river with regular bed forms. Relatively low-density gradients due to an initial salt pulse concentration of 1.55 kg m^{-3} applied in the experiment were found to modulate significantly the pore-water flow and solute transport in the riverbed. Such density gradients increased downward flow and solute transport in the riverbed by factors up to 1.6. This resulted in a 12.2% increase in the total salt transfer from the water column to the riverbed over the salt pulse period. As the solute pulse passed, the effect of the density gradients reversed, slowing down the release of the solute back to the river water by a factor of 3.7. Numerical modeling indicated that these density effects intensified as salt concentrations in the water column increased. Simulations further showed that the density gradients might even lead to unstable flow and result in solute fingers in the bed of large bed forms. The slow release of solute from the bed back to the river led to a long tail of solute concentration in the river water. These findings have implications for assessment of impact of pollution events on river systems, in particular, long-term effects on both the river water and riverbed due to the hyporheic exchange.

1. Introduction

Unintended release of toxic chemicals due to industrial accidents has caused a number of major river pollution incidents worldwide. On 1 November 1986, a major fire at a chemical warehouse in Schweizerhalle on the Rhine River above Basel led to the release of 1246 tons of highly toxic pesticides into the river. These toxic substances formed a plume 70 km long, which moved downstream causing a devastating impact on the river system, especially for the river's biota [*Mossman et al*., 1988; *Giger*, 2009]. The accident killed the majority of fish over a downstream distance of 160 km [*Liu*, 2008; *Giger*, 2009]. On 30 January 2000, a tailings dam at a mining site broke and released 100,000 m^3 of tailings pulp, heavily contaminated with cyanide and cyanide complexes, into the Lapus and Somes tributaries of the Tisa River in central Europe. The polluted water overflowed and flooded a large area in the basin from the Tisa River to the downstream Danube River, killing all aquatic organisms, birds, wild boars, and other land animals as well as plants. In the polluted areas, some unique biological species became extinct [*Laszlo et al*., 2000; *Michnea and Gherhes*, 2001; *Liu*, 2008]. On 13 November 2005, the release of nearly 100 tons of benzene substances into the Songhua River occurred due to an explosion at an aniline production factory of the Jilin Petrochemical Corporation, China. The accident led to shutting down of the potable water supply to Harbin City located 500 km downstream from the accident site [*Fu et al*., 2008; *Dai et al*., 2010].

To assess the pollution problems caused by these accidents, it is important to determine how the released chemicals are transported downstream in the river system. Many researchers have conducted tracer experiments in natural rivers to study how the solute concentration in the river water changed after the tracer was released as a pulse input [*Bencala et al*., 1990; *Runkel et al*., 1998; *Worman et al*., 1998; *Haggerty et al*., 2002; *Gooseff et al*., 2005; *Worman et al*., 2005; *Marion et al*., 2008]. *Eylers* [1994] and *Elliott and Brooks* [1997] conducted laboratory experiments in a flume under similar pulse input conditions. The measurements of tracer concentrations in the river water at a distance from the release point during these experiments showed a general trend of rising and declining concentrations corresponding to the approaching and

passing of the tracer plume. If the tracer plume underwent advective and diffusive/dispersive transport, the concentration profile would follow the normal distribution. However, local concentrations measured during the tracer experiments tended to show asymmetrical profiles with longer concentration-declining phases than rising phases [*Worman et al*., 1998; *Worman et al*., 2005]. Tails of low concentrations (but higher than the background level) persisted in these profiles for long periods after the plumes had passed. For example, 1 month after the incident in Danube River, elevated chemical concentrations were still detectable in the river downstream from the accident location [*Laszlo et al*., 2000; *Michnea and Gherhes*, 2001; *Nguyen et al*., 2009]. This phenomenon has implications for a proper assessment of the pollution impact on both the river water quality and the habitat within the river [*Worman*, 1998], especially if the pollutant remains toxic even at low concentrations.

Investigations of river pollution incidents have tended to focus on solute concentrations in the river water [*Fu et al*., 2008], and neglect the transport of solutes into the riverbed and their later release back to the overlying surface water. The temporary storage provided by the riverbed can lead to tailing of the solute concentration of the river water as observed in the field and laboratory experiments [*Bencala and Walters*, 1983; *Bencala et al*., 1990; *Elliott and Brooks*, 1997; *Worman et al*., 1998; *Worman et al*., 2005]. Note that although this study examines only transient storage provided by the riverbed, other processes can also contribute to it, for example, mass exchange with "surface dead zones" in the river [*Briggs et al*., 2009; *Stewart et al*., 2011].

The transfer of solutes to the bed and the release back to the river water, broadly termed hyporheic exchange, has been studied extensively [*Elliott and Brooks*, 1997; *Boano et al*., 2007, 2011; *Cardenas and Wilson*, 2007a, 2007c; *Cardenas et al*., 2008; *Hester et al*.,2013; *Zhu et al*.,2014]. In particular, pore-water flow driven by pressure gradients resulting from interactions between flowing river water and bed forms was demonstrated to be a key mechanism for hyporheic exchange and solute transport in the riverbed (Figure 1) [*Cardenas and Wilson*, 2007a; *Gibbes*, 2007]. Density gradients, due to variations of solute concentrations, are also involved in this transport problem. Most previous studies assumed that such density gradients are small due to relatively low solute concentrations and hence negligible [*Marion et al*., 2003; *Salehin et al*., 2004; *Jin et al*., 2010]. However, *Boano et al*. [2009] and *Jin et al*. [2011] showed that even small density gradients resulting from the presence of solutes at low concentrations can modify the hyporheic flow significantly. These studies considered a continuous, nearly constant solute input to the river. In that case, the density gradients are upward, and enhance the downward flow and net solute transfer from the river to the bed.

In the case of a solute pulse input such as that involved in the pollution accidents described above, similar density effects to those shown by *Boano et al*. [2009] and *Jin et al*. [2011] are expected during the initial phase as the solute plume in the river water approaches and passes through the location of concern. However, as the plume moves further downstream, the infiltrated solute is still in the bed, and so the local solute concentration in the river water is lower than that in the pore-water. Consequently, the density gradient is downward, which would be expected to constrain the upward flow and hence the release of solute back to the river water. However, to what extent this negative effect may lead to modifications of the flow and solute transport in the bed is unclear. Moreover, how do the negative and positive density effects combine to influence the overall hyporheic exchange and solute concentration in the river water, in particular the long tail?. This study was designed to address these questions through laboratory experiments and numerical simulations.

2. Laboratory Experiments and Numerical Simulations

2.1. Laboratory Experiments

The experimental setup was the same as used in *Jin et al*. [2010], and was based on a circulating flume system that physically models a river with a bed including uniform triangular bed forms (Figure 1e). River sand from the Yangtze River, with $d_{50} = 0.30$ mm, was used. The bulk porosity was measured using the water evaporation method [*Chinese National Standard*, 1999] as 0.33 and the saturated hydraulic conductivity, measured using the constant-head method [*Chinese National Standard*, 1999], was found to be 8.84×10^{-4} m s^{-1}. The sand was thoroughly cleaned before all experiments following methods described by *Jin et al*. [2010].

The experimental methods were the same as applied in *Jin et al*. [2010], including the techniques used to make the uniform triangular bed forms and withdraw pore-water samples from two vertical arrays of

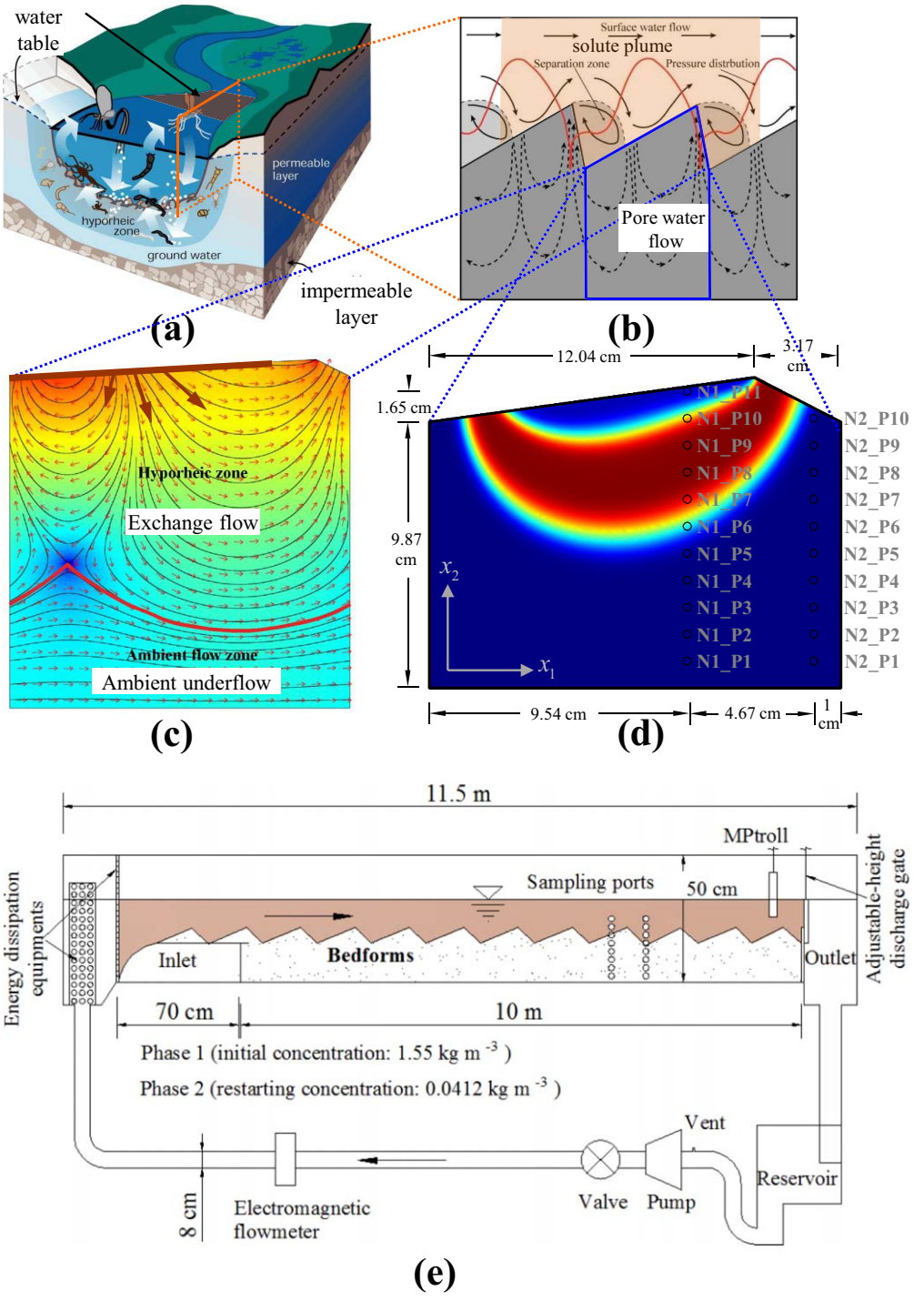

Figure 1. (a) Schematic diagram of the hyporheic zone in a river/stream system (after *Alley et al*. [2002]). (b) Pore-water flows beneath a repeating bed form subject to unidirectional flow (after *Gibbes* [2007]). The pressure distribution (red line) along the riverbed surface, induced by the current-bedform interaction, generates pore-water flow in the streambed. (c) Pore water flow in the streambed. Arrows (with equal lengths) show the direction of pore water flow. The color scale represents the natural logarithm (for better visualization) of the pore-water flow rate, with warm colors for high rates and cool for low rates. Streamlines are represented by black lines. The red streamline divides the streambed into two parts: the hyporheic zone and the ambient underflow zone. (d) Development of a solute plume as a result of solute transport in the bed during a pollution event with pulse-like input of the pollutant to the river. Sampling ports (two columns, N1 and N2) were preinstalled for pore-water sampling during the experiment. (e) The experimental setup based on a closed, recirculating sand flume. The surface water, initially polluted, was replaced after a preset period (pulse period) with deionized water to simulate the pulse input condition for the river water.

sampling ports (with 1 cm intervals between neighboring ports, Figure 1d) at the stoss and lee slopes of a bed form.

NaCl was used as the tracer, the concentration of which was measured through electrical conductivity (EC) for pore-water samples, using the DDSJ-308A probe manufactured by Shanghai Precision and Scientific Instrument Company. A self-logging probe (MPTROLL 9500) was installed to measure EC (salt concentration) and temperature in the river water at the end of the flume every 4 min throughout the experiment. The average flow velocity and water depth in the river water were 11.62 cm s^{-1} and 9.31 cm, respectively.

To simulate the pulse input condition, the experiment started with an initial solute (salt) concentration of 1.55 kg m^{-3} in the river water and zero in the riverbed. Note that this salt concentration is relatively low (compared with, for example, the typical ocean water salt concentration, 35 kg m^{-3}). The experiment ran for a pulse time (T) of 3 h before the overlying river water was then drained and replaced quickly with deionized water to start the second phase of the experiment under the same surface water flow condition. After the replacement of the river water, a small amount of salt residual existed in the overlying water at a very low concentration of 0.041 kg m^{-3}. For the drainage and water replacement, there was little or no surface water flow over the bed and hence little exchange across the bed surface occurred. The rapid change of the river water concentration, although not entirely representing the real condition, simulated a nearly "square" pulse input. This pulse input comprised two phases. The first phase started with tracer injection and lasted until the surface water was replaced with deionized water. During this phase, net tracer transfer from the overlying water to streambed occurred. The second phase covered the remaining period of the experiment, during which net tracer transfer from the streambed to overlying water occurred. Because of the circulating flume (a closed system) that was used, the concentration in the overlying water varied with time in both phases as a result of solute transfer across the bed surface.

2.2. Numerical Simulations

A one-way sequential coupling method was used to link two models for simulating the river water flow, and pore-water flow and solute transport in the riverbed, respectively. First, the river water flow was computed using the CFD package FLUENT based on the Reynolds-averaged Navier-Stokes equations together with the k-ω turbulence closure scheme [*Jin et al*., 2010]. The predicted pressure at the riverbed surface was then input into a COMSOL-based model as boundary conditions to drive coupled pore-water flow and solute (salt) transport in the bed [*Jin et al*., 2010].

Density-dependent flow in the bed was described by [*COMSOL*, 2006]:

$$\rho S_f \frac{\partial h_f}{\partial t} + \theta \frac{\partial \rho}{\partial C}\frac{\partial C}{\partial t} + \nabla \cdot \left[-\rho K_f \left(\nabla h_f + \frac{\rho - \rho_f}{\rho_f} \nabla x_2 \right) \right] = 0, \tag{1}$$

where h_f (m), the equivalent freshwater hydraulic head, is given by $p/\rho_f g + x_2$ with p (Pa) being the pore-water pressure, ρ_f (1000 kg m^{-3}) the freshwater density, and x_2 (m) the vertical coordinate directed upward; C (kg m^{-3}) is the solute concentration; ρ (kg m^{-3}) is the fluid density; S_f (m^{-1}) is the equivalent freshwater specific storativity, representing storage due to compressibility of the fluid and porous medium; t (s) is the time; θ is the porosity; and K_f (m s^{-1}) is the equivalent freshwater hydraulic conductivity. The fluid density was modeled as:

$$\rho = \rho_f + \frac{\partial \rho}{\partial C} C = \rho_f + \gamma C, \tag{2}$$

where γ is 0.7143 for the salt solution applied in the experiments [*Langevin et al*., 2003].

The second term on the left-hand side of equation (1) represents change in storage due to concentration variations and is likely to dominate the compressible storage term due to the relatively small compressibility of the river sand used in the study [*Jin et al*., 2010]. Coupled with the pore-water flow, the salt solute transport in the porous bed was determined using [*COMSOL*, 2006]:

$$\frac{\partial C}{\partial t} = \frac{\partial}{\partial x_i}\left(D_{ij}\frac{\partial C}{\partial x_j} - u_i C \right), \tag{3}$$

where C (kg m^{-3}) is the solute concentration, u_i ($i = 1, 2$, m s^{-1}) is the pore-water flow velocity component in the x_i ($i = 1, 2$) direction (Figure 1d),

$$u_1 = \frac{-\rho K_f}{\theta}\frac{\partial h_f}{\partial x_1} \tag{4}$$

$$u_2 = \frac{-\rho K_f}{\theta}\left(\frac{\partial h_f}{\partial x_2} + \frac{\rho - \rho_f}{\rho_f}\right) \tag{5}$$

D_{ij} ($m^2\ s^{-1}$) is the component of the 2-D dispersion coefficient tensor:

$$D_{ii} = \alpha_L \frac{u_i^2}{|u|} + \alpha_T \frac{u_j^2}{|u|} + D_e \tag{6}$$

$$D_{ij} = D_{ji} = (\alpha_L - \alpha_T)\frac{u_i u_j}{|u|} + D_e \tag{7}$$

Here, α_L (m) is the longitudinal dispersivity and α_T (m) is the transverse dispersivity. The absolute value $|u| = \sqrt{u_1^2 + u_2^2}$ is the magnitude of the pore water flow velocity. D_e ($m^2\ s^{-1}$) is the effective molecular diffusion coefficient in the porous medium.

The initial and boundary conditions for both the river water flow model, and pore-water flow and solute transport model followed *Jin et al*. [2010, 2011] as shown in Figure 2, simulating the conditions in the laboratory experiments. The predicted pressure at the riverbed surface from the river water flow simulation was converted to the equivalent freshwater head based on the density of the river water, which was then applied to set the boundary condition at the top of the bed for the pore-water flow simulation. Since the solute concentration and hence the density of the river water change with time as a result of solute exchange across the bed surface, the converted equivalent freshwater head varied temporally. Periodic boundary conditions were applied to the lateral (vertical) boundaries for velocity, pressure, concentration, and solute flux (Figure 2). A no-flow condition was applied at the bottom boundary [*Jin et al*., 2010].

As mentioned in the last section, the pulse input applied in the laboratory experiment comprised two phases. In simulating the first phase of the experiment, the initial solute concentration in the pore water within the bed was set to zero and to $C_0 = 1.55$ kg m^{-3} for the overlying river water. In simulating the second phase, the initial solute concentration in the river water was changed to 0.041 kg m^{-3} (measured residual concentration after replacing the river water with deionized water) and the initial solute concentration in the pore water was kept the same as that simulated at the end of the first phase. In the laboratory experiment, the concentration in the overlying water varied with time in both phases as a result of solute transfer across the bed surface. In the simulation, the time-varying concentration (C_t) at a given time step was calculated based on the simulated solute transfer rates from previous time steps and used to specify the solute concentration at the bed surface as part of the boundary condition (Figure 2c): for phase 1, the calculation was according to the following equation [*Jin et al*., 2010]:

$$C_t = \frac{C_0 V_s - B\int_{A_b} \theta C(x_1, x_2, t)\, dA}{V_s} \tag{8}$$

where V_s ($m\ s^{-1}$) is the total volume of water in the flume system excluding pore water in the streambed, $C(x_1, x_2, t)$ (kg m^{-3}) is the simulated solute concentration of pore water at location $C(x_1, x_2)$ (kg m^{-3}) at time t, B is the width of the river (flume width in the experiment), A (m^2) is the area (on the $x_1 - x_2$ plane), and A_b (m^2) is the total area of the bed. For phase 2, C_t (kg m^{-3}) was calculated from:

$$C_t = \frac{C_1 V_s + B\int_{A_b} \theta C(x_1, x_2, T)\, dA - B\int_{A_b} \theta C(x_1, x_2, T)\, dA}{V_s} \tag{9}$$

where C_1 (kg m^{-3}) is the residual concentration in the river water at the beginning of phase 2, i.e., after the river water was replaced with deionized water.

Simulations were conducted to examine the flow and solute transport in the bed according to the conditions applied in the laboratory experiment without (case 1) and with (case 2) density effects (Table 1). A reference simulation with no density effects incorporated was also conducted for comparison. The aim of the simulations was to ascertain the effects of density gradients on pore-water flow and solute transport in the bed, and the overall solute exchange between the river water and bed. Further simulations were then conducted to explore the density effects under a wider range of conditions, in particular, with increased solute

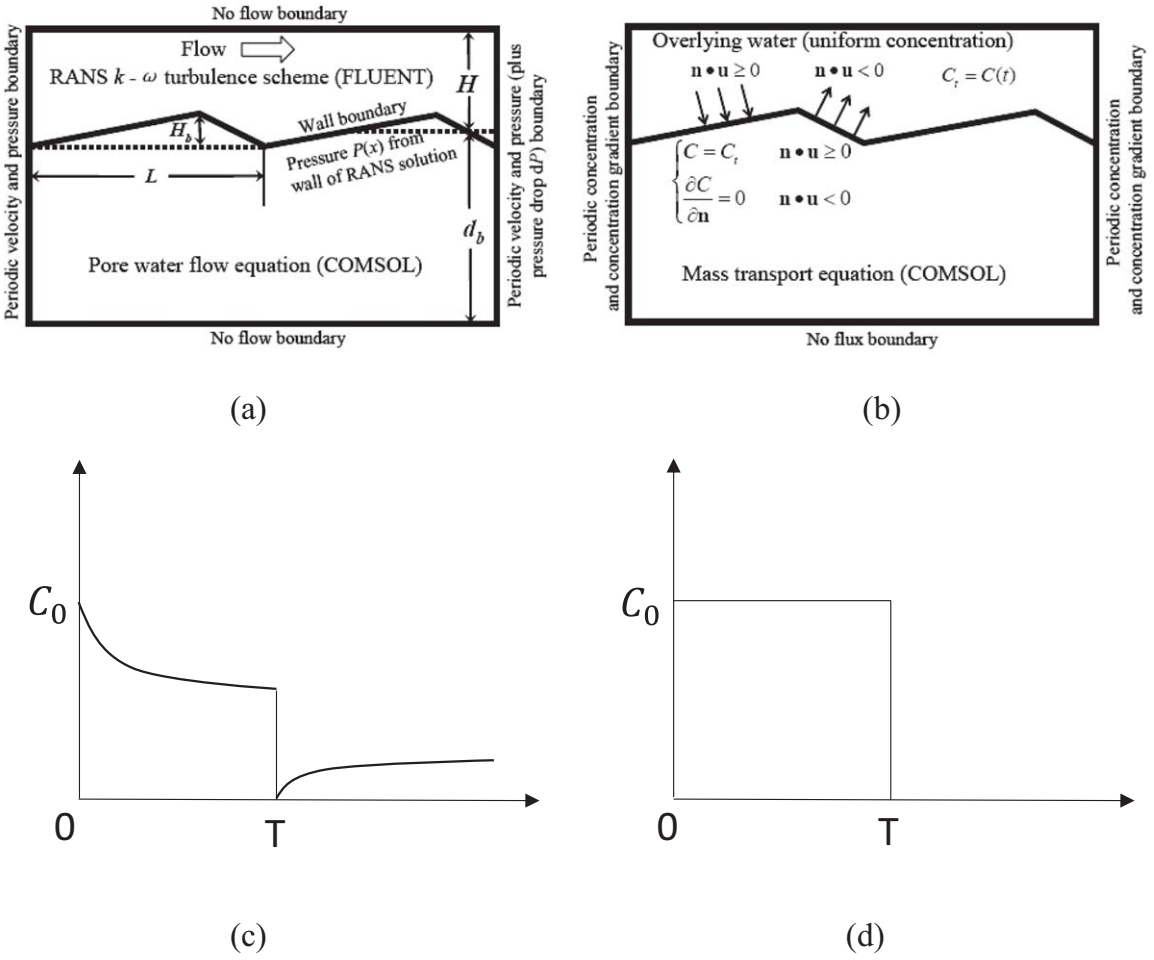

Figure 2. Schematic of simulation domain and boundaries. (a) Water flow (after *Cardenas and Wilson* [2007a]). L, H, H_b, and d_b are bedform length, average water depth of overlying water, bedform height, and average depth of streambed, respectively. (b) Solute transport. Uniform concentration is assumed in the overlying water. (c) Concentration in the overlying water varying with time under the experimental condition. This was used to define the boundary condition at the bed surface for simulations of the experiment. C_0 and T are the initial concentration and pulse time, respectively. (d) Concentration in the overlying water varying with time. This was used in the additional simulations under conditions of different solute input concentrations and based on a field scale model.

input concentrations (larger density gradients) and an enlarged simulation domain to simulate a field condition (Table 2). For these additional simulations, a square pulse input was applied in order to generalize the results (Figure 2d).

3. Results and Discussion

3.1. Temporal Variation of Solute Concentration in the Overlying Water: Experimental Conditions

The changes of the solute concentration in the river water result from the overall solute exchange across the riverbed surface, which is caused by pore-water flow and solute transport in the bed. In the following, we examine how the solute concentration in the river water varied with time in phases 1 and 2 (Figure 3).

In the first phase ($t \leq 180$ min), the solute concentration in the river water decreases due to transfer of solute to the bed. The concentration decline is rapid initially because the solute enters the bed through the shallow and fast circulation cells (Figure 3a), and gets stored there [*Cardenas and Wilson*, 2007a, 2007b, 2007c]. As time goes on, the solute traveling through these shallow cells returns to the river and the net transfer is mainly due to solute moving through deeper and slower circulation cells, which slows down the overall solute transfer rate. These trends are evident in the experiment as well as numerical simulations (Figure 3a).

Numerical simulations with and without density effects underpredict the decline of the solute concentration in the river water, i.e., underprediction of the net transfer of solute to the bed. However, the numerical model performs better with density effects included, predicting lower concentrations that match the

Table 1. Simulation Cases Based on the Experimental Conditions (Laboratory Scale)

Case No.	θ	K (m s^{-1})	Density Effects	Bed Form Length (cm)	Bed Form Height (cm)	Stoss Length (cm)	Streambed Depth (cm)
1	0.33	8.84×10^{-4}	No	15.21	1.65	10.70	12.04
2	0.33	8.84×10^{-4}	Yes	15.21	1.65	10.70	12.04

measurements reasonably well. Comparison between the experimental and numerical results indicates that in the first phase, density gradients enhance the downward flow and solute transport in the riverbed, and hence the net transfer of solute to the bed, which leads to lower solute concentrations in the river water. These results are consistent with those of *Jin et al*. [2011].

During the second phase, the solute concentration in the river water (which was replaced with deionized water) will increase as transfer of solute back to the river water takes place. Contrary to the behavior observed in the first phase, the concentration in the river water rose relatively quickly at the beginning because of the initial exchange (flushing) in the shallow area where fast circulating hyporheic flow take place (Figure 3b). The rising trend attenuated with time as the solute moved slowly out from the deep area of the bed. Comparison between the experimental and numerical results indicates again that the density effects are important and constrain the initial release of solute back to the river water. Without density effects incorporated, the model overpredicts the initial solute release and hence the rise of the solute concentrations. The constraining effects of density gradients on the solute release also leads to a long tail of slowly rising solute concentrations in the river water. Based on the simulation results, we determined the elapsed time by which 90% of the solute in the riverbed had been released back to the river water during the second phase for cases 1 and 2 as shown in Figure 3b. Consistent with the experimental results (Figure 3b), the 90% release time simulated with the density effects included (2371 min after the pulse time T) is much longer than that simulated without the density effects (470 min after the pulse time T). This time lag reflects clearly the long tail in the solution concentration of river water due to the density effects, as observed in the experiment.

3.2. Measured and Simulated Solute Concentration Profiles in the River Bed: Experimental Conditions

During the experiments, pore-water samples were taken from two vertical arrays of sampling ports shown in Figure 1d. N1 was located in the stoss slope area of a bed form where river water entered the bed and N2 in the lee slope area of the bed form where pore water exited the bed (both at the bed surface). The measured solute concentrations of the collected pore-water samples are shown in Figure 4 together with numerical predictions.

During the first phase ($t \leq 180$ min), the solute was transported into the bed as shown by the concentration profile at N1 (Figure 4a). Although a solute front appeared to move downward in the profile, the actual solute transport was not wholly vertical but instead followed circulating pathways driven by the hyporheic flow with both horizontal and vertical components (Figures 1c and 1d). The numerical model was able to predict reasonably well the measured concentration profiles despite underprediction of the downward movement of the solute front. With the density effects incorporated, the model performed better and predicted faster movement of the solute (front) into the bed, indicating the enhancement of downward porewater flow and solute transport due to upward density gradients. For example, the downward flow at point P7 along array N1 (Figure 1d) was enhanced by a factor of 1.6 compared with the normal flow velocity (with

Table 2. Values of Model Parameters Used in the Field-Scale Simulations[a]

Parameter	Value	Parameter	Value
Average velocity for overlying water (U)	0.2 m s^{-1}	Porosity (θ)	0.33
Average water depth for overlying water (H)	0.5 m	Water density (ρ_f)	1000 kg m^{-3}
Bed form length (L)	1 m	Water dynamic viscosity (μ)	0.001 Pa s
Bed form height (H_b)	5 cm	Longitudinal dispersivity (α_L)	0.001m
Stoss length (L_c)	0.9 m	Transverse dispersivity (α_T)	0.0001 m
Streambed depth (d_b)	1 m	Effective diffusion coefficient (D_e)	10^{-9} m^2 s^{-1}
Intrinsic permeability (κ)	9.02^{-10} m^2	Solute concentration in overlying water ($C=C_0$)	1∼10 kg m^{-3}

[a]These parameter values for the field-scale model are based on the work of *Cardenas and Wilson* [2006] and *Cardenas et al.*[2008].

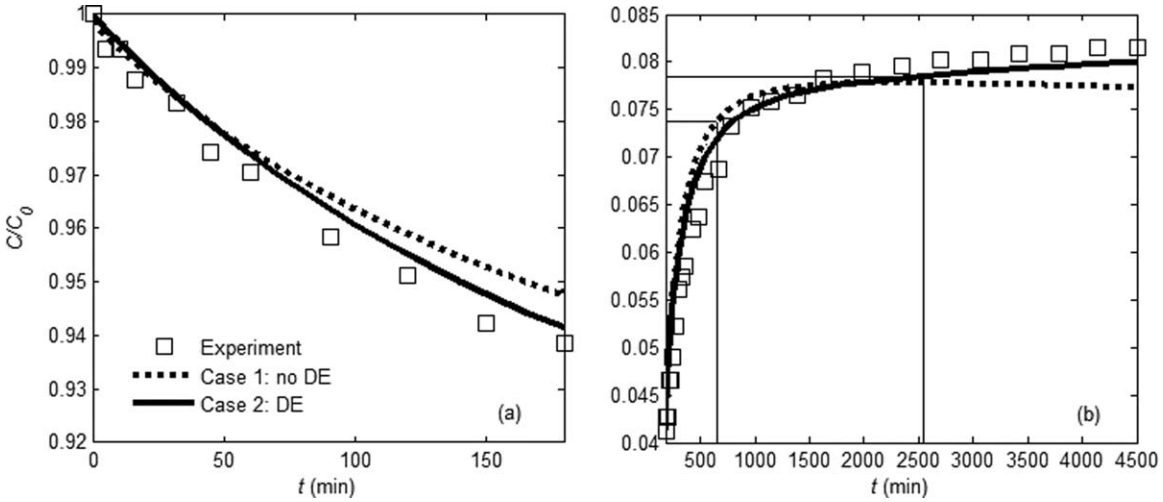

Figure 3. Comparison of experimental data and modeled solute concentration in the overlying river water: (a) phase 1 over the pulse input period ($t \leq 3$ h); (b) phase 2 after the pulse input. DE = density effect. Note that the time for replacing the overlying water with deionized water between phase 1 and 2 is neglected in Figure 3b. The two cross lines indicate the elapsed time by which 90% of the maximum net transfer solute into the bed had been released back to the river water for cases 1 (on the left) and 2 (on the right). Thus the origin of the time axis (horizontal axis) is the same in Figures 3a and 3b.

no density effects) around elapsed time 180 min (shown later in Figure 6a). The sampling ports at N2 were located downstream of those at N1 along the circulating transport pathways and thus were expected to receive the solute later. Indeed, no solute was detected along the N2 sampling array during phase 1 (and hence no results are shown for N2 in this phase).

As the river water was switched to "clean" water, the second phase of solute transport led to a quick response of the solute concentration profile at N1 (Figure 4b). An upper solute front formed with local saline water replaced by clean river water flowing relatively quickly through the shallow circulation cells. At the same time, solute in the deep area continued to move downward through deep, slow circulation cells. This led to formation of a solute pulse in the concentration profile, which moved downward with time (Figure 4b). With density effects included, the model predictions overall matched the measured concentrations well, in particular, in the lower area where the density gradient enhanced flow and solute transport downward. At point P2 along array N1 (Figure 1d) around elapsed time 1000 min, the downward flow was enhanced by a factor of 2.2 (shown later in Figure 6a). Without density effects, the predicted solute pulse disappeared before reaching the deep area near the bottom boundary, in contrast to the measurements.

The concentration profile at N2 in the outlet area (where pore water and solute flow back into the river at the bed surface) responded differently, with a time lag that corresponds to the solute travel time through the circulation cells (Figure 4c). Elevated solute concentrations appeared in the shallow area at N2 after the river water was replaced with clean water (i.e., phase 2). Subsequently, a solute pulse also formed and moved down on the concentration profile, similar to the trend observed at N1. However, the pulse appeared to be wider, reflecting the large differences in solute (or clean water) travel time along different circulation cell pathways. Density effects are also demonstrated by the comparison between the experimental and numerical results for N2.

3.3. Density Effects on Flow and Solute Transport in the Hyporheic Zone: Experimental Conditions

Both measured and predicted solute concentrations in the river water and pore water presented above suggest that density effects played an important role in affecting the pore-water flow and solute transport in the riverbed. Since the pore-water flow could not be measured easily during the experiment, we used the modeling results to analyze how flow and solute transport are coupled, i.e., how the density gradients affects pore-water flow, which in turn modifies the solute transport.

Figure 5 shows the flow field and solute plume in the riverbed at different times for both cases (with and without density effects), based on the simulation results. The solute plume appeared to move downward as time went on. This movement is mainly due to advective transport of solute driven by

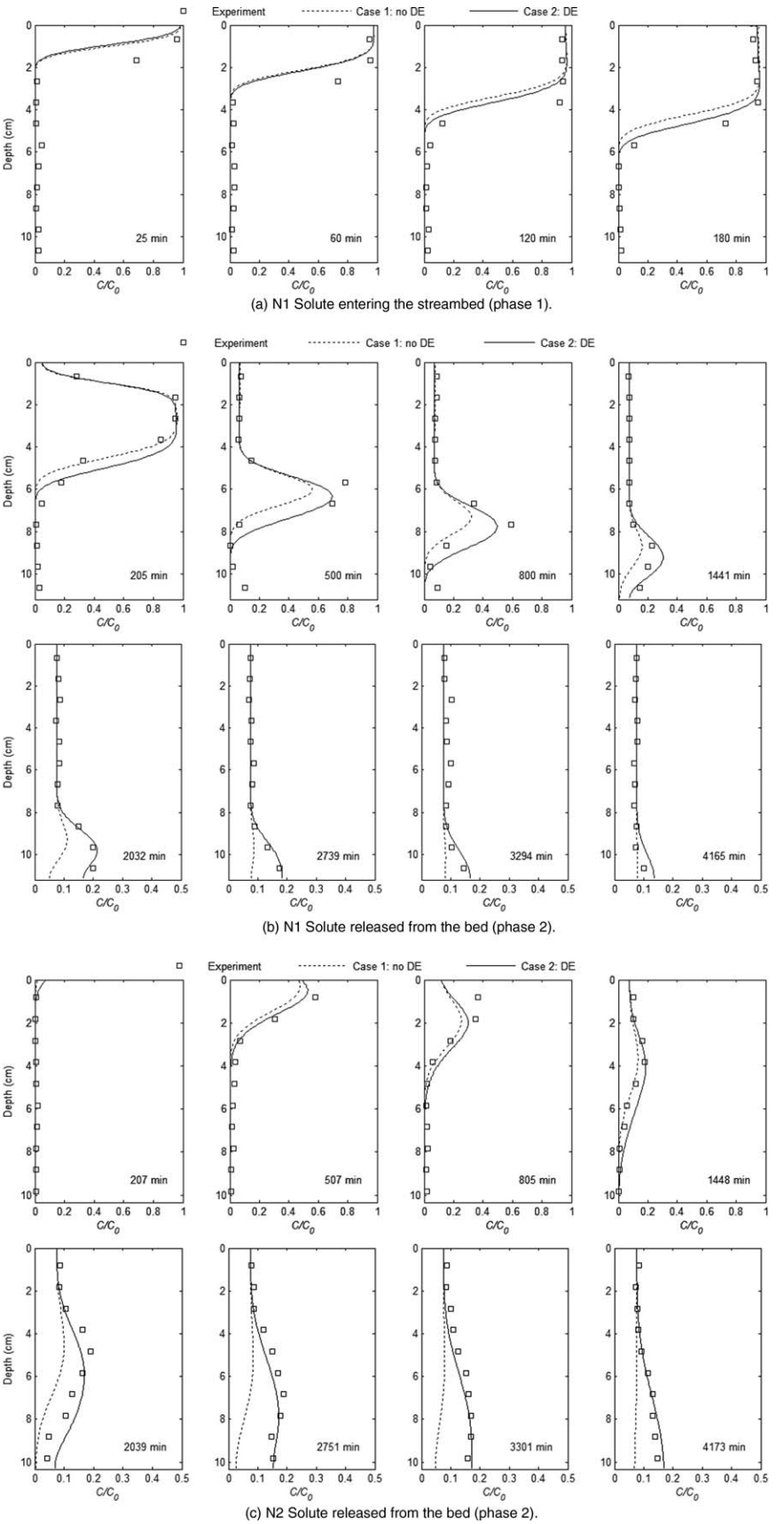

Figure 4. Temporal variations of solution concentration profiles along two sampling arrays at N1 and N2, respectively.

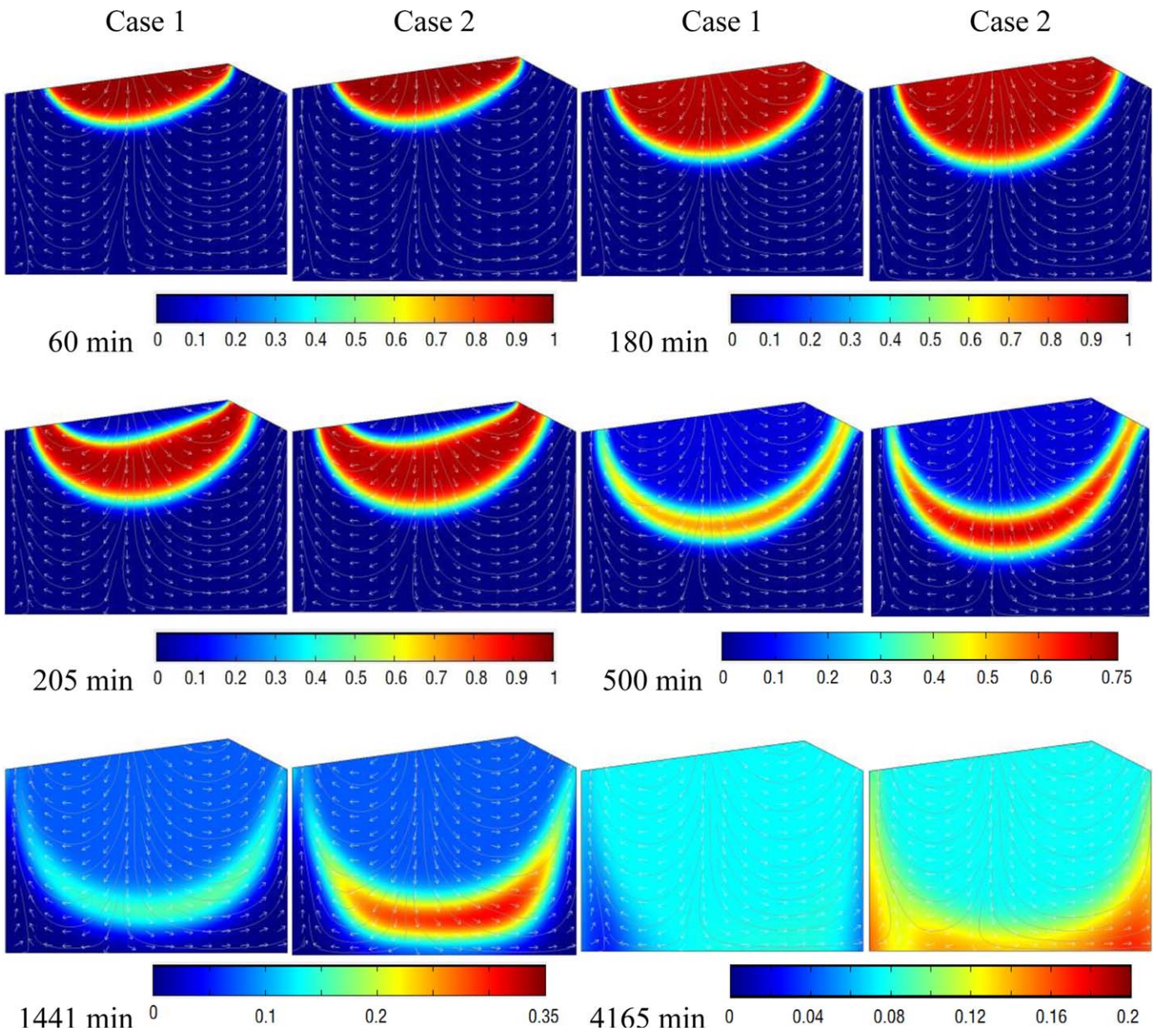

Figure 5. Flow field showing pore-water circulations and solute plume formed during and after the pollution event. Cases 1 and 2 are without and with density effects included, respectively. The color scale represents solute concentration (*C*) in the bed, with warm colors for high concentration and cool for low concentration.

two pore-water circulations in the upstream and downstream direction, respectively. Again, differences in the behavior of the solute plume between the two cases (with/without density effects) are evident. In particular, density effects lead to a more extensive solute plume that moves further down to reach the bottom boundary of the bed, compared with the solute simulated with no density effects included. This is also evident in the solute concentration profiles along array N2 as shown in Figure 4c, particularly for elapsed times 2751, 3301, and 4173 min. Due to the large difference in the flow magnitude between the shallow and deep areas, only the flow direction is shown in the figure. The results show that the solute plume, as it moved downward and induced density gradients on both the upper and lower edges, hardly changed the flow direction. However, the magnitude of local flows in areas where concentration variations and density gradients existed was subjected to changes in a dynamic way as the solute plume travelled downward, as demonstrated in the simulation results of flow velocity and solute concentrations along the N1 and N2 arrays.

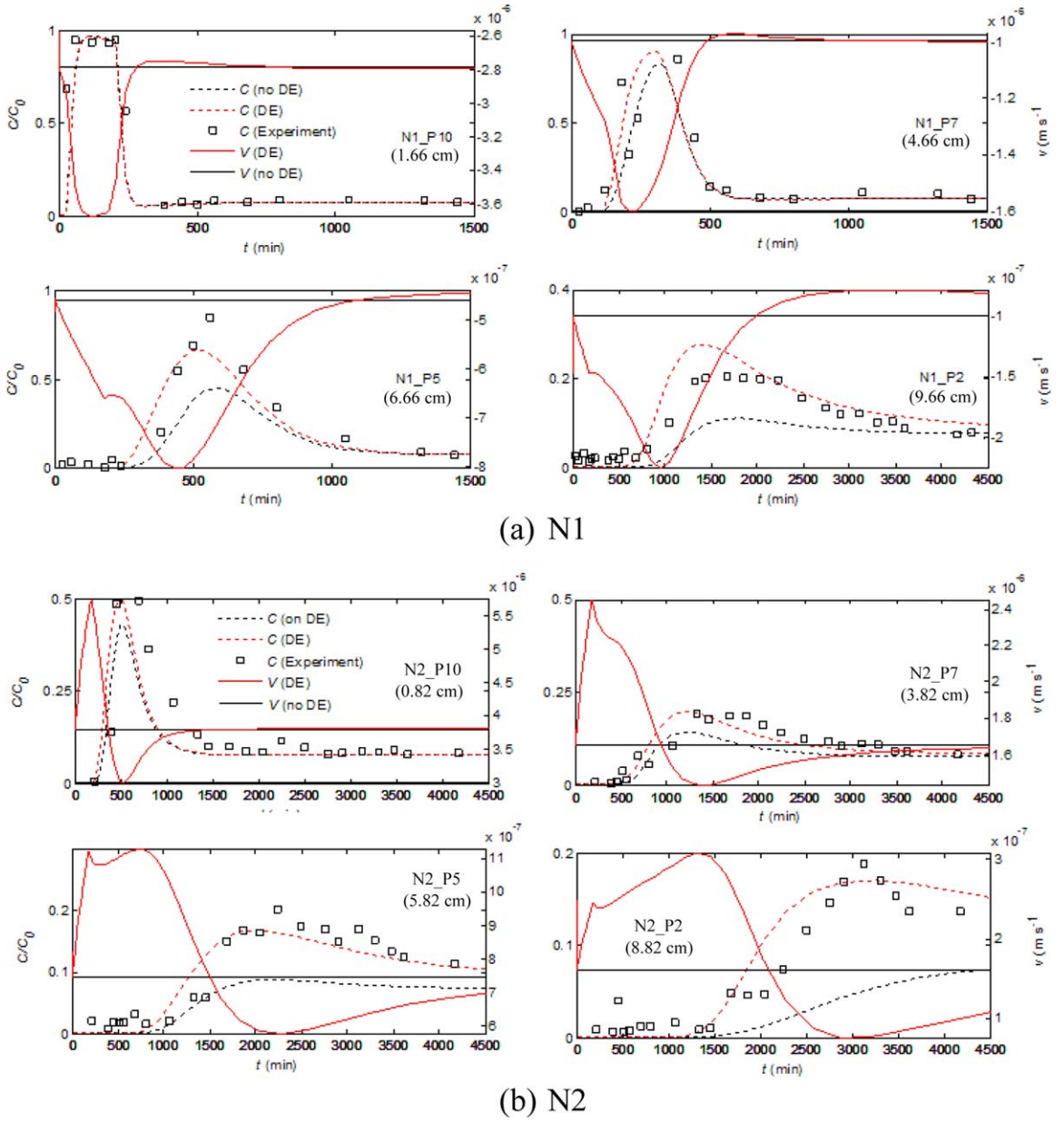

Figure 6. Flow and solute transport coupling at different sampling ports on the N1 and N2 arrays. Only vertical flow is shown. Note that the flow velocity is shown on the right-hand side axis of each figure. Negative velocity values indicate downward flow and vice versa. The numbers in the brackets below the port numbers indicate the depths of the ports (from the bed surface).

For all the ports at N1 (Figure 1d), the vertical flow velocity (negative values) was directed downward due to the array's location in the "inlet" area. The vertical flow clearly responded to the solute plume (Figure 6a). As the solute front approached any of these ports and generated an upward density gradient, the local flow speeded up significantly (e.g., by a factor of 1.6 at point N1_P7 around elapsed time 180 min). The increase of the flow speed was due to the local density gradient. As the solute plume passed, the vertical flow slowed down as the local, now downward density gradient became resistant to the downward flow. This slowing down effect was minor in the shallow area (ports N1_P10 and N1_P7, Figure 6a) and diminished as the plume moved down further (i.e., the vertical flow speed returned to the level predicted by the model without density effects incorporated). The behavior of flow slowing down was more visible in the deep area (ports N1_P5 and N1_P2) and lasted for the rest of the experiment. This was because in the area of these two ports, local downward density gradient persisted for a long time as shown in Figure 5.

The vertical flow velocity in the "outlet" area of N2 (Figure 1d), directed upward, also varied in response to the movement of the solute plume (Figure 6b). The changes were, however, different from those at the ports of N1. The local upward flow speed at these N2 ports started to rise before the approach of the solute front. This speed increase was in response to the flow intensification (e.g., increased vertical downward flow at the N1 ports) in the upstream section of the circulation cell (a flow tube), as required by flow continuity. Note that a port at N2 was linked to an N1 port at a higher elevation, which experienced flow intensification earlier. As the local solute plume approached the port, the local upward flow slowed down with the speed declining below the normal level (no density effect) due to the upward density gradient associated with the plume. For example, the speed declined by 47.1% at point N2_P2 around elapsed time 3000 min (Figure 6b). Subsequently, with the passing of the solute plume, the flow speed recovered relatively quickly to the ambient level in the shallow area but in the deep area, the recovery was gradual and incomplete (with the speed remaining below the normal level).

3.4. Simulated Density Effects in the Hyporheic Zone: Conditions of Increased Density Contrasts at Laboratory and Field Scale

To further explore the density effects on the hyporheic processes, simulations were conducted with a range of solute input concentrations (C_0 = 1, 2, 3, 4, 5, 6, 7, 8, 9, and 10 kg m^{-3}) based on the laboratory-scale model (i.e., the experimental setup) as well as a field-scale model (Table 2). The high input concentrations simulated typically occur near the spill in reality. As the contaminant is transported downstream in the river, the concentration decreases, as represented by the lower concentration cases. For the purpose of simplicity and generality, a square pulse input (Figure 2d) with an initial concentration (C_0) in the river water over the pulse period (T) was applied for each simulation. In the simulations, the pulse period was set to 3 h for the laboratory-scale model and 24 h for the field-scale model.

3.4.1. Effect of Density on Flow and Solute Transport in the Hyporheic Zone

The flow field and solute plume in the bed versus time from the laboratory-scale and field-scale models are shown in Figures 7 and 8, respectively. Only results for C_0 = 5 and 10 kg m^{-3} are presented here and results for other solute input concentrations are included in supporting information. Density effects on the hyporheic flow and solute transport processes increase with the increased density contrast. Significant changes of flow directions (shown by the vector plots) and speeds (as indicated by the plume movement) in the laboratory model are evident at all times in both phases 1 and 2 (Figure 7). Note that under the experimental condition (with C_0 = 1.55 kg m^{-3}), density effects lead to changes of flow speed but little modification of flow direction (Figure 5). As the solute plumes move down to the deep area, density effects become more profound, and result in local circulation. In the deep area, the flow is weak and much less affected by the head variations on the bed surface, and hence the density effects are more important.

In the field-scale model, flow instability occurred with solute fingers formed during phase 1, especially in the case of C_0 = 10 kg m^{-3} (Figure 8). Fingers formed even in the lee slope area where outflow of pore water would take place if no density effects were present. The unstable flow provided a rapid transport mechanism for the solute with fingers reaching the deep area much faster than the stable solute plume. The solute fingers formed in the case of C_0 = 10 kg m^{-3} reached the domain bottom at depth 1 m at elapsed time 12 h when the front of the stable solute plume in the case of C_0 = 2 kg m^{-3} arrived only at a depth of 31 cm (Figure 8 and supporting information Figure S2). This stable plume did not reach the domain bottom until elapsed time 541.7 h (supporting information Figure S2). While the fingers were localized features that interspersed the bed, we show in the next sections that they lead to increased net solute transfer from the river to the bed. These fingers persist over phase 2 and affect the release of solute back to the river. Note that the formation and behavior of the fingers depend on the solute input concentration (initial density contrast) as shown in supporting information Figure S2.

3.4.2. Effect of Density on Net Solute Transfer Across the Bed Surface

As demonstrated in the above section, density gradients influence the flow and solute transport in the hyporheic zone significantly. The density effects are expected to cause marked changes of net solute transfer across the bed surface. To examine how such changes depend on the solute input concentration, we calculated, based on the simulation results, the temporal variation of total solute mass that accumulates in the bed (m) for all simulated cases:

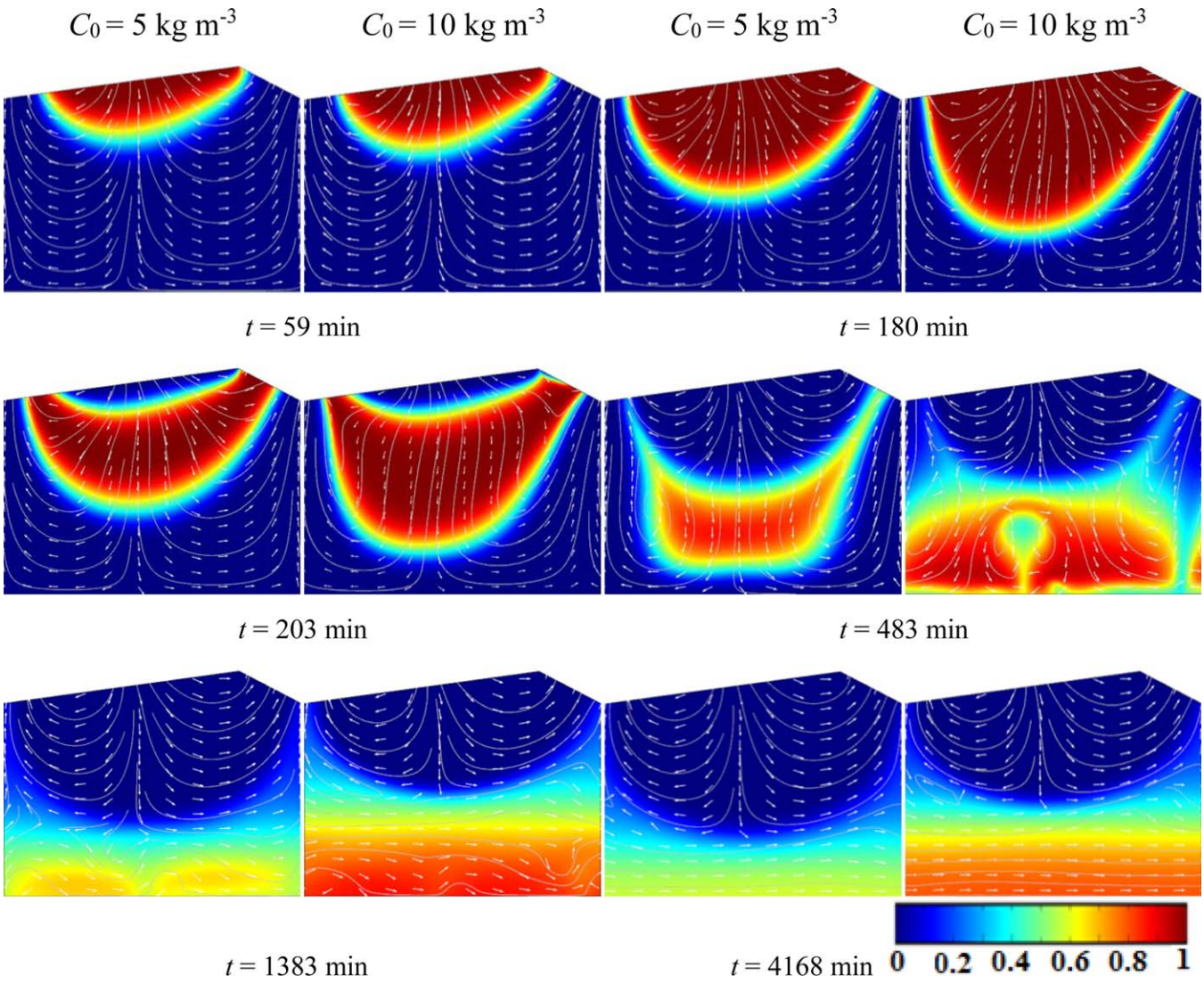

Figure 7. Simulated flow field of pore water and solute plume formed in the bed during and after the pollution event based on the laboratory scale model. Only two cases with $C_0 = 5$ and 10 kg m^{-3}, respectively, are shown here and the results for other cases can be found in Figure S1 (supporting information). The color scale represents solute concentration (C) in the bed, with warm colors for high concentration, and cool for low concentration. The concentration in the streambed is normalized by C_0.

$$m = B\theta \int\int_A C(x_1, x_2, t)\mathrm{d}A \tag{10}$$

To facilitate the analysis of the results for different solute input concentrations, we normalized m by $B\theta AC_0$ (solute mass stored in the bed with pore-water solute concentration equal to C_0), i.e.,

$$m^* = \frac{\int\int_A C(x_1, x_2, t)\mathrm{d}A}{A\,C_0} \tag{11}$$

We nondimensionalized time (t) by the pulse time period T (= 3 h for all the cases based on the laboratory-scale model and 24 h for the cases based on the field scale model), i.e.,

$$t^* = t/T \tag{12}$$

The results plotted in Figure 9 show large variations among the different cases with different solute input concentrations. For example, the maximum m^* in the case with $C_0 = 10$ kg m^{-3} is approximately double that in the case with no density effects (i.e., $C_0 = 0$ kg m^{-3}, Figure 9a). Without density effects, the

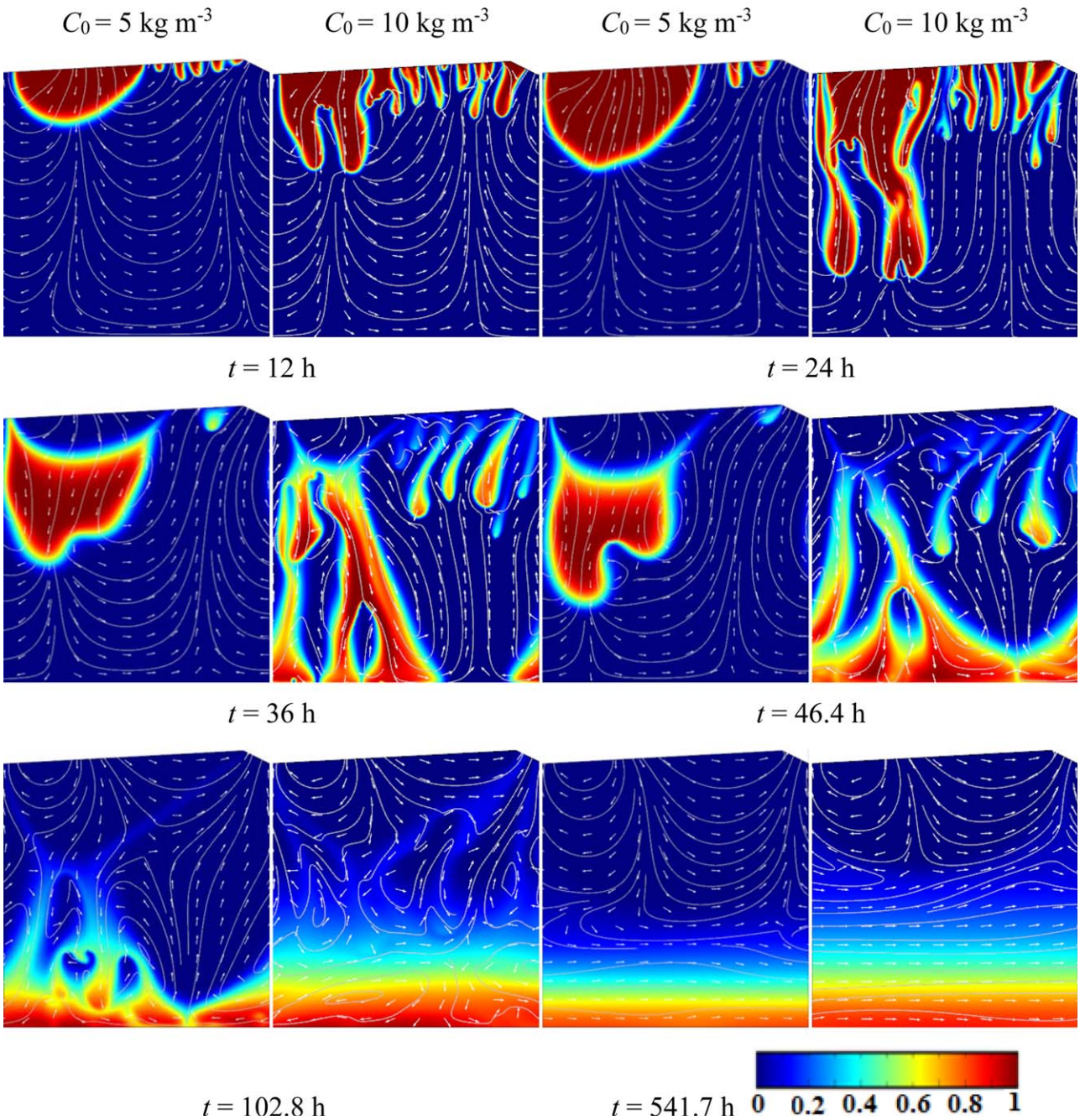

Figure 8. Simulated flow field of pore water and solute plume formed in the bed during and after the pollution event based on the field-scale model. Only two cases with $C_0 = 5$ and 10 kg/m^3, respectively, are shown here and the results for other cases can be found in Figure S1 (supporting information). The color scale represents solute concentration (C) in the bed, with warm colors for high concentration, and cool for low concentration. The concentration in the streambed is normalized by C_0.

normalized mass transfer (m^*) would be invariant for different values of C_0 as shown by the NDE (No Density Effect) curve in the figure. With density included, there is a near-linear trend in the maximum m^* ($m^*_{max} = m^*(t = T)$) as it varies with C_0 for both the laboratory-scale and field-scale model (Figure 10). Given that the pulse period was kept a constant in each case, this trend suggests that the average speed of the overall (downward) solute movement in phase 1 increased linearly with C_0.

To examine the release of solute from the bed during the second phase, we calculated another normalized quantity (m^{**}) by dividing m^* by m^*_{max}, i.e., $m^{**} = m^*/m^*_{max}$. This allows comparison of the release rates among the cases with different C_0 values. As shown in Figure 11, larger density gradients

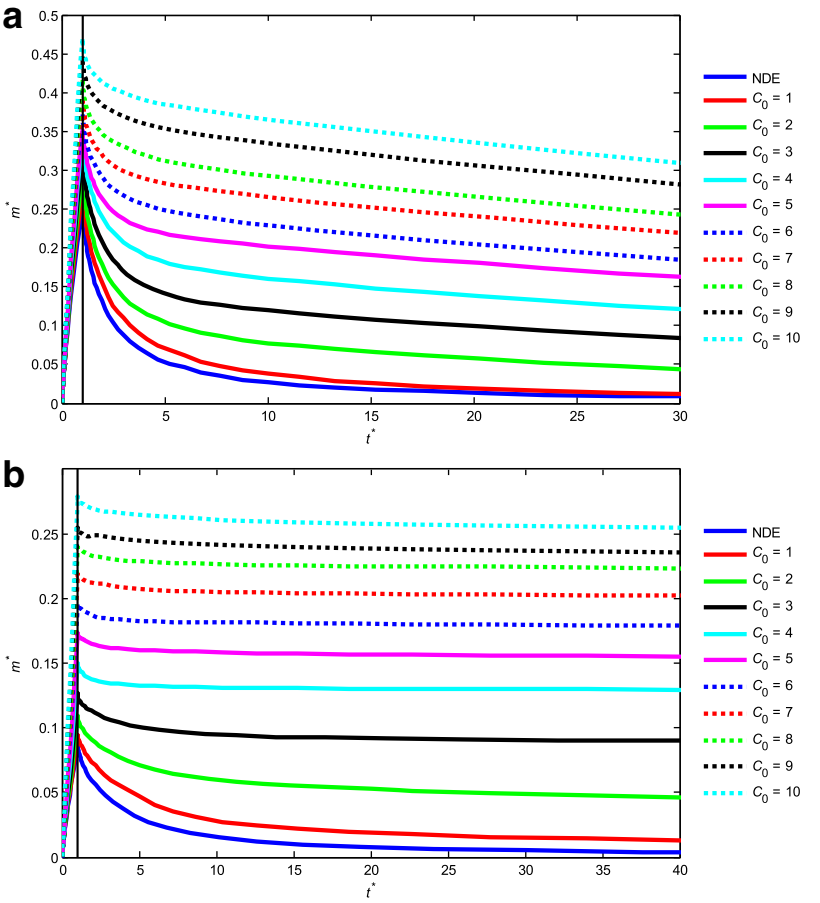

Figure 9. Normalized solute mass (m^*) in the bed varying with nondimensional time (t^*) with different C_0 (kg m^{-3}): (a) based on the laboratory-scale model; and (b) based on the field-scale model.

associated with increased solute input concentrations slowed down significantly the solute release from the bed. It took a longer time from m^{**} to decline to a low value (e.g., 10%) for larger C_0. We determined the time when m^{**} reached 10%, i.e., t^*_{10}, and plotted it in Figure 12. The results show that for both the laboratory-scale and field-scale models, t^*_{10} increased with C_0, indicating that the attenuating effects of density gradients on the solute release from the bed during the second phase intensifies as the solute input concentration increases.

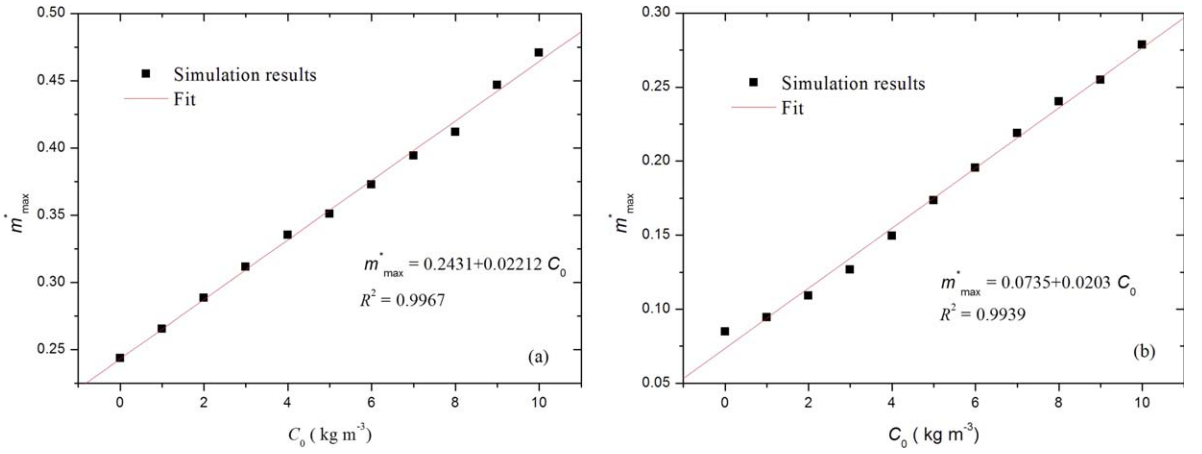

Figure 10. Maximum normalized solute mass in the bed (m^*_{max}) as it varies with C_0 (kg m^{-3}): (a) based on the laboratory-scale model; and (b) based on the field-scale model.

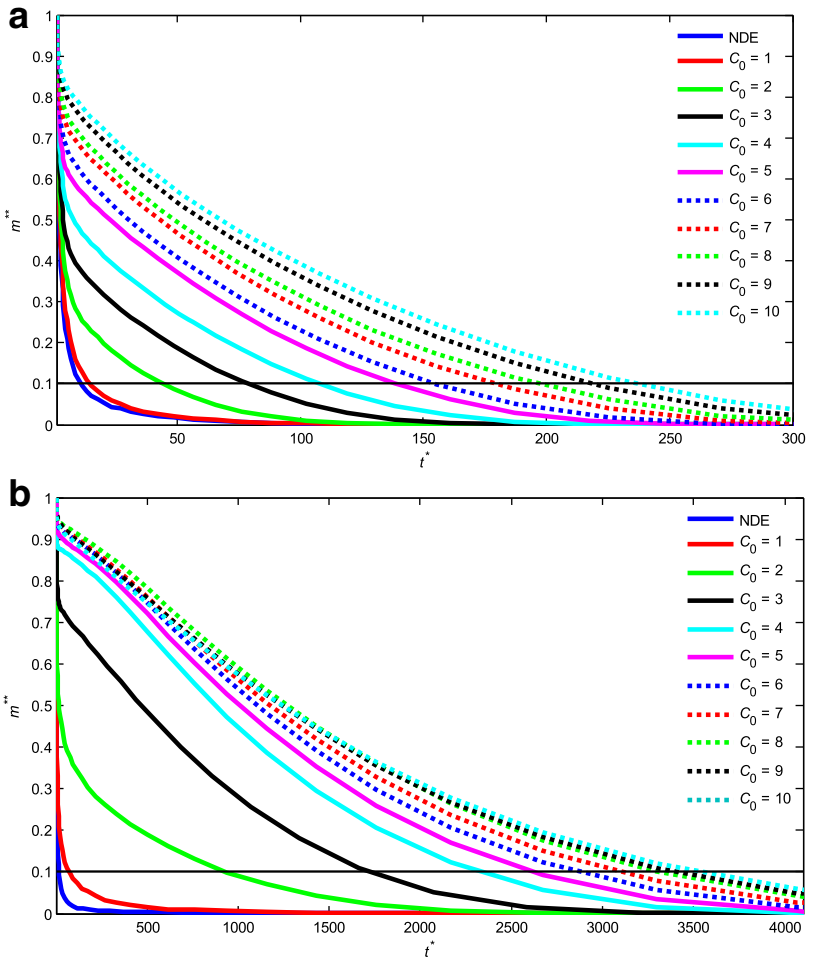

Figure 11. Variations of m^{**} with t^* showing the process of solute release from the bed for cases with different C_0 (kg m^{-3}): (a) based on the laboratory-scale model; and (b) based on the field-scale model.

The effects are twofold as discussed in section 3.4.1. First, the transport of solute from the shallow area out of the bed is impeded due to the constraining effects of (negative) density gradients on the upward flow and solute transport. Second, the lower part of the solute plume continues to move downward assisted by the local positive density gradients. This effect also slowed down the overall release of solute from the bed. With a simple square pulse condition specified on the bed surface, the model did not simulate the feedback

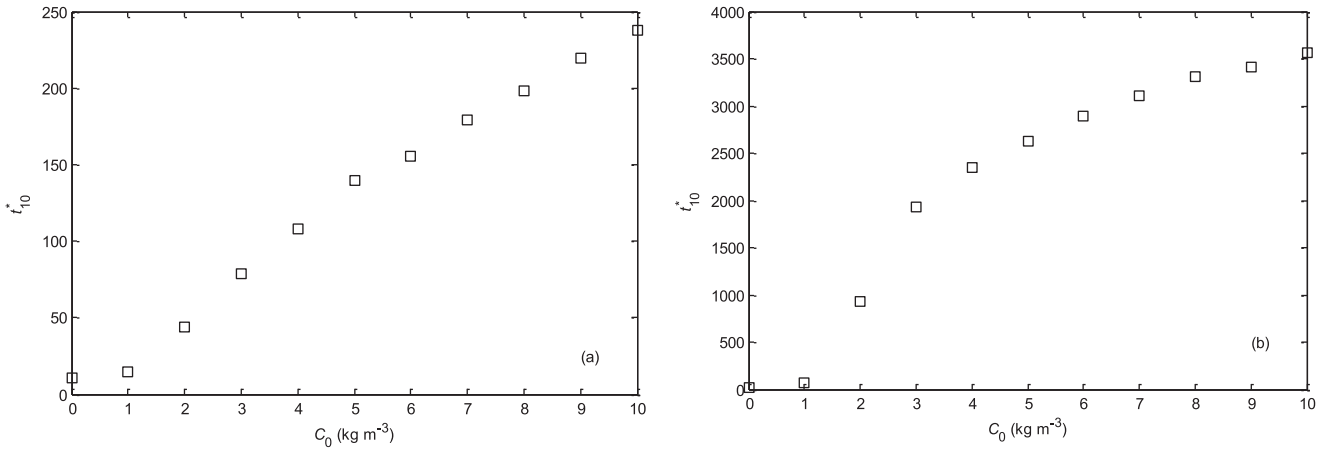

Figure 12. Time (t^*) when m^{**} reached 10%: (a) based on the laboratory-scale model; and (b) based on the field-scale model.

of released solute on the river water quality as shown in the laboratory experiment. However, the demonstrated reduction of solute release from the bed due to density gradients on solute release from the bed can lead to a long-lasting presence of solute in the river water, albeit at low concentration. As indicated by the time of 10% solute residual in the riverbed, the presence of solute in the river water affected by density gradients in the cases with $C_0 = 5$ and 10 kg m^{-3} can last 144 and 195 times longer than that in the case with no density effect, respectively.

4. Concluding Remarks

We conducted a laboratory experiment and numerical simulations to examine density effects on flow and solute transport in the hyporheic zone under conditions of solute pulse input to river water. The results from both the experiment and numerical simulations demonstrate changes of pore-water flow direction and speed induced by density gradients, which in turn modify the solute transport behavior in the bed and exchange across the bed surface. These density effects lead to enhanced solute transfer from the river water to the bed (by 12.2% under the experimental condition) as the solute pulse approaches and passes. It also constrains solute release back to the river water after the solute pulse passes. These effects intensify linearly with increased solute input concentrations. The simulations showed that at the field-scale density effects may even lead to unstable flow in the hyporheic zone, resulting in formation of solute fingers that penetrate the bed at a faster pace than the stable downward movement of the solute plume.

The findings presented here were based on a specific hyporheic flow condition driven by hydraulic head variations along the bed due to interactions between flow river water and bed forms. However, the demonstrated density effects are likely to be a general characteristic of the river system. These effects can lead to more extensive solute transfer (by 12.2% under the experimental condition) to the riverbed during a pollution incident and afterward slower release of the pollutant from the bed back to the river water (by factors up to 195 in the simulated cases under realistic conditions), causing a secondary pollution problem for the river system. Therefore, the hyporheic exchange subject to the influence of density gradients should be considered in environmental impact assessment of pollution incidents in rivers, especially the long-term impact.

The numerical simulations were extended to cover a wider range of conditions than applied in the laboratory experiment. While these simulations generated more insights into the density effects, further experiments should be conducted to examine the simulated behaviors and phenomena, for example, the unstable flow. Simulations and theoretical analyses are also needed to determine the critical condition for the initiation of the unstable flow. These issues present directions for future research to advance our understanding of the hyporheic processes in relation to river water quality and eco-functionality.

Acknowledgments
This research was supported by the Natural Science Foundation of China (51109059, 51239003, 51125034), National Basic Research Program of China (973 Program, 2012CB417005, 2011CB403303), Basic Research Programs (Natural Science Foundation) of Jiangsu Province (BK2011749), the Specialized Research Fund for the Doctoral Program of Higher Education (20110094120004), and Program for Changjiang Scholars and Innovative Research Team in University (IRT1233). The authors acknowledge the assistance provided by Xiaoquan Yang, Ming Chen, Kai Xie, and Qihao Jiang during the experiments and simulations. Data used in the analysis presented in the paper can be obtained by sending a request to the corresponding author (hwtang@hhu.edu.cn).

References

Alley, W., R. Healy, J. LaBaugh, and T. Reilly (2002), Flow and storage in groundwater systems, *Science*, *296*(5575), 1985–1990.
Bencala, K., D. McKnight, and G. Zellweger (1990), Characterization of transport in an acidic and metal-rich mountain stream based on a lithium tracer injection and simulations of transient storage, *Water Resour. Res.*, *26*(5), 989–1000.
Bencala, K. E., and R. A. Walters (1983), Simulation of solute transport in a mountain pool-and-riffle stream: A transient storage model, *Water Resour. Res.*, *19*(3), 718–724, doi:10.1029/WR019i003p00732.
Boano, F., R. Revelli, and L. Ridolfi (2007), Bedform-induced hyporheic exchange with unsteady flows, *Adv. Water Resour.*, *30*(1), 148–156.
Boano, F., D. Poggi, R. Revelli, and L. Ridolfi (2009), Gravity-driven water exchange between streams and hyporheic zones, *Geophys. Res. Lett.*, *36*, L20402, doi:10.1029/2009GL040147.
Boano, F., R. Revelli, and L. Ridolfi (2011), Water and solute exchange through flat streambeds induced by large turbulent eddies, *J. Hydrol.*, *402*(2011), 290–296.
Briggs, M. A. G., M. N. Gooseff, C. D. Arp, and M. A. Baker (2009), A method for estimating surface transient storage parameters for streams with concurrent hyporheic storage, *Water Resour. Res.*, *45*, W00D27, doi:10.1029/2008WR006959.
Cardenas, M. B., and J. L. Wilson (2006), The influence of ambient groundwater discharge on exchange zones induced by current-bedform interactions, *J. Hydrol.*, *331*(1-2), 103–109.
Cardenas, M. B., and J. L. Wilson (2007a), Hydrodynamics of coupled flow above and below a sediment-water interface with triangular bedforms, *Adv. Water Resour.*, *30*(3), 301–313.
Cardenas, M. B., and J. L. Wilson (2007b), Exchange across a sediment-water interface with ambient groundwater discharge, *J. Hydrol.*, *346*(3-4), 69–80.
Cardenas, M. B., and J. L. Wilson (2007c), Dunes, turbulent eddies, and interfacial exchange with permeable sediments, *Water Resour. Res.*, *43*, W08412, doi:10.1029/2006WR005787.
Cardenas, M. B., J. L. Wilson, and R. Haggerty (2008), Residence time of bedform-driven hyporheic exchange, *Adv. Water Resour.*, *31*(10), 1382–1386.
Chinese National Standard (Ed.) (1999), *Standard for Soil Test Method, GB/T50123-1999* [in Chinese], 7–21, China Planning Press, Bejing.
COMSOL (2006), *FEMLAB 3.3 Multiphysics Modeling: User's Guide*, 14–91, Burlington, Mass.

Dai, Y., N. Terui, Y. Lin, S. Tanaka, K. Jin, Y. Hirama, M. Teduka, M. Zhang, X. Shen, and B. Fugetsu (2010), Determination of nitrobenzene in water and ice samples collected from the Songhua River after an explosion of a petrochemical plant and investigation on enclosing behavior of nitrobenzene into ice, *Anal. Sci.*, *26*(4), 519–523.

Elliott, A. H., and N. H. Brooks (1997), Transfer of nonsorbing solutes to a streambed with bed forms: Theory, *Water Resour. Res.*, *33*(1), 123–136.

Eylers, H. (1994), Transport of adsorbing metal ions between stream water and sediment bed in a laboratory flume, *Rep. KH-R-56*, Calif. Inst. of Technol., Pasadena, Calif.

Fu, W., H. Fu, K. Sk tt, and M. Yang (2008), Modeling the spill in the Songhua River after the explosion in the petrochemical plant in Jilin, *Environ. Sci. Pollut. Res.*, *15*(3), 178–181.

Gibbes, B. (2007), Pore water exchange processes in offshore intertidal sandbanks, PhD thesis, The Univ. of Queensland, Australia.

Giger, W. (2009), The Rhine red, the fish dead: The 1986 Schweizerhalle disaster, a retrospect and long-term impact assessment, *Environ. Sci. Pollut. Res.*, *16*(1), 98–111.

Gooseff, M. N., J. LaNier, R. Haggerty, and K. Kokkeler (2005), Determining in-channel (dead zone) transient storage by comparing solute transport in a bedrock channel-alluvial channel sequence, Oregon, *Water Resour. Res.*, *41*, W06014, doi:10.1029/2004WR003513.

Haggerty, R., S. M. Wondzell, and M. A. Johnson (2002), Power-law residence time distribution in the hyporheic zone of a 2nd-order mountain stream, *Geophys. Res. Lett.*, *29*(13), doi:10.1029/2002GL014743.

Hester, E. T., K. I. Young, and M. A. Widdowson (2013), Mixing of surface and groundwater induced by riverbed dunes: Implications for hyporheic zone definitions and pollutant reactions, *Water Resour. Res.*, *49*, 5221–5237, doi:10.1002/wrcr.20399.

Jin, G., H. Tang, B. Gibbes, L. Li, and D. A. Barry (2010), Transport of nonsorbing solutes in a streambed with periodic bedforms, *Adv. Water Resour.*, *33*(11), 1402–1416.

Jin, G., H. Tang, L. Li, and D. A. Barry (2011), Hyporheic flow under periodic bedforms influenced by low-density gradients, *Geophys. Res. Lett.*, *38*, L22401, doi:10.1029/2011GL049694.

Langevin, C., W. Shoemaker, and W. Guo (2003), MODFLOW-2000, the US Geological Survey modular ground-water model: Documentation of the SEAWAT-2000 version with the variable-density flow process (VDF) and the integrated MT3DMS transport process (IMT), *U.S. Geol. Surv. Open File Rep.*, *3*(426), 1–43.

Laszlo, F., B. Csanyi, and P. Literathy (2000), Cyanide and heavy metals accidental pollution in the Tisza river basin: Consequences on water quality monitoring and assessment, in *Monitoring Tailor-Made III: Information for Sustainable Water Management, Proceedings of the International Workshop Monitoring Tailor-Made: III, 25–28 September 2001*, 65–70, Nunspeet, Netherlands.

Liu, Yan. (2008) Strategies for managing accidental pollution incidents. Master thesis, Jilin University, Changchun, China.

Marion, A., M. Bellinello, I. Guymer, and A. Packman (2003), Effect of bed form geometry on the penetration of nonreactive solutes into a stream bed, *Water Resour. Res.*, *39*(1), 1209, doi:10.1029/2001WR000264.

Marion, A., M. Zaramella, and A. Bottacin-Busolin (2008), Solute transport in rivers with multiple storage zones: The STIR model, *Water Resour. Res.*, *44*, W10406, doi:10.1029/2008WR007037.

Michnea, A., and I. Gherhes (2001), Impact of metals on the environment due to technical accident at Aurul Baia Mare, Romania, *Int. J. Occup. Med. Environ. Health*, *14*(3), 255–259.

Mossman, D., J. Schnoor, and W. Stumm (1988), Predicting the effects of a pesticide release to the Rhine River, *J. Water Pollut. Control Fed.*, *60*(10), 1806–1812.

Nguyen, H., M. Braun, I. Szaloki, W. Baeyens, R. Van Grieken, and M. Leermakers (2009), Tracing the metal pollution history of the Tisza River through the analysis of a sediment depth profile, *Water. Air. Soil Pollut.*, *200*(1), 119–132.

Runkel, R. L., D. M. McKnight, and E. D. Andrews (1998), Analysis of transient storage subject to unsteady flow: Diel flow variation in an Antarctic stream, *J. N. Am. Benthol. Soc.*, *17*(2)143–154.

Salehin, M., A. I. Packman, and M. Paradis (2004), Hyporheic exchange with heterogeneous streambeds: Laboratory experiments and modeling, *Water Resour. Res.*, *40*, W11504, doi:10.1029/2003WR002567.

Stewart, R. J., W. M. Wollheim, M. N. Gooseff, M. A. Briggs, J. M. Jacobs, B. J. Peterson, and C. S. Hopkinson (2011), Separation of river network-scale nitrogen removal among the main channel and two transient storage compartments, *Water Resour. Res.*, *47*, W00J10, doi:10.1029/2010WR009896.

Worman, A. (1998), Analytical solution and timescale for transport of reacting solutes in rivers and streams, *Water Resour. Res.*, *34*(10), 2703–2716.

Worman, A., J. Forsman, and H. Johansson (1998), Modeling retention of sorbing solutes in streams based on tracer experiment using Cr-51, *J. Environ. Eng.*, *124*(2), 122–130.

Worman, A., B. Klove, P. Wachniew, P. Czuprynski, and A. Packman (2005), Tracer test in Hobol creek, Norway, under different flow conditions, *Acta Geophys. Pol.*, *53*(4), 517.

Zhu H., P. Cheng,and D. Wang (2014), Relative roles of resuspended particles and pore water in release of contaminants from sediment, *Water Sci. Eng.*,*7*(3), 344–350.